ELSEVIER

Polymer 41 (2000) 2627–2632

polymer

Skin/core micro-structure in viscose rayon fibres analysed by X-ray microbeam and electron diffraction mapping

M. Müller[a,*], C. Riekel[a], R. Vuong[b], H. Chanzy[b]

[a]*European Synchrotron Radiation Facility, B.P. 220, F-38043 Grenoble Cedex, France*
[b]*Centre de Recherches sur les Macromolécules Végétales, CERMAV-CNRS, affiliated with the Université Joseph Fourier, B.P. 53, F-38041 Grenoble Cedex 9, France*

Received 22 January 1999; received in revised form 28 April 1999; accepted 9 June 1999

Abstract

The skin/core morphology of viscose fibres was analysed by X-ray microbeam diffraction applied to individual fibres and by electron diffraction on longitudinal fibre cross-sections. Both techniques yield position-resolved diffraction maps which reveal that (1) the cellulose molecules are far better aligned in the fibre skin than in their core and (2) there is no significant difference between skin and core concerning both mean crystallite size and crystallinity. Comparing the X-ray microbeam diffraction with electron diffraction techniques there is a clear advantage for X-ray experiments as they lead to quantitative results on individual fibres without the necessity of elaborate specimen sectioning and handling.

Keywords: Microbeam X-ray diffraction; Electron diffraction; Viscose

1. Introduction

The spinning process has a strong influence on the structure and properties of regenerated cellulose fibres such as those of viscose rayon. Unlike many other textile fibres, a number of viscose fibres benefit from a “skin” and a “core” that are the result of certain chemical conditions in the spinning bath [1]. Such skin/core structure (where the skin may amount up to 50% of the cross-section area) yields strong and tough yarns, which combine high strength with high elongation. These interesting physical properties are due to the different characteristics of the fibre skin and core. The different structures of the skin and core regions of viscose fibres are also reflected in their dying ability. Depending on the experimental conditions, it is possible to stain the skin and not the core or vice-versa and therefore visualise the skin/core morphology by optical microscopy on the fibre cross-sections [2].

Despite a good characterisation of the skin and core materials with respect to their macroscopic properties [3]—such as density, tensile strength, or water absorption—the structural differences on the supermolecular and morphological organisation level of cellulose in the two different regions have not yet been investigated directly. However, these differences are the key for an understanding of the mechanical fibre properties.

Fibres from regenerated cellulose (cellulose II) have a semi-crystalline structure and, therefore, are composed of crystallites together with more or less disordered (“amorphous”) regions. Typical dimensions of the cellulose II crystallites are 4–6 nm in diameter and 10–20 nm in length [4,5]. *Crystallinity*, *crystallite size* and the *orientation* of the crystallites with respect to the fibre axis are believed to vary between the skin and core structure [1,3]. Since the thickness of a skin layer is just a few micrometers, a probe providing information on the nanostructure in combination with microscopic position resolution is needed to confirm the micro-structural features of these fibres. The technique of microbeam diffraction mapping—using either X-rays [6] or electrons [7]—fulfils these requirements: from a selected small area of the sample—corresponding to the beam size of the order of 1–2 μm in diameter—a diffraction pattern can be obtained which contains information on crystallite dimension, orientation and overall crystallinity.

In the present work, we have investigated individual viscose fibres possessing a skin/core structure using both micron-size X-ray and electron beams. With these two techniques, significantly different diffraction diagrams were obtained from viscose skin and core respectively, independently of the radiation used. A comparison between the

* Corresponding author. Tel.: +33-4-7688-2724; fax: +33-4-7688-2542.
E-mail address: mmueller@esrf.fr (M. Müller)

0032-3861/00/$ - see front matter
PII: S0032-3861(99)00433-4

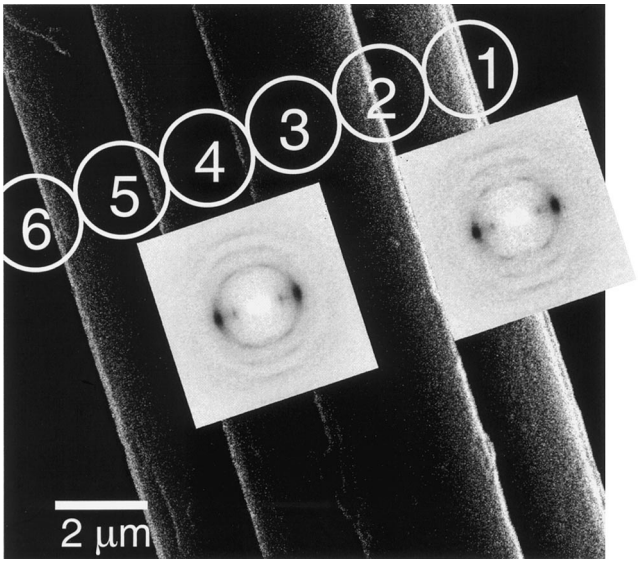

Fig. 1. SEM image of a single Fibro® rayon fibre (prepared by Snigireva, ESRF). The serrated surface is characteristic for a viscose fibre possessing a skin layer. The numbered circles show schematically the positions of the measurements with the X-ray microbeam (the diameter of the circles corresponds to the beam size). The two diffraction diagrams (insets), from fibre edge (position 1) and centre (position 4), are scaled to the same integrated intensity.

technique of X-ray versus that of the electrons in view of quantitative findings and necessary efforts in sample preparation is also emphasised.

2. Experimental

2.1. Sample preparation and characterisation

Viscose fibres (F295, Fibro®) were provided by Courtaulds Research and Technology, Coventry, UK. For the X-ray experiments, a stereomicroscope was used in sample preparation. A single fibre was isolated from a fibre bundle and glued across the hole of a metal ring (diameter 4 mm). After the experiment, the fibre was investigated in a scanning electron microscope (SEM). In Fig. 1, which is a typical SEM image, the fibre has a diameter of 9 μm and shows the characteristic serrated surface of a viscose fibre possessing a skin layer [1].

To prepare thin sections for the electron diffraction experiments, a small fibre bundle was embedded in Nanoplast resin following a standard embedding method [8]. The blocks were ultra-sectioned along the fibre axis with a LKB Ultratome IV equipped with a 35° Diatome diamond knife. The sections were mounted on carbon coated 200 mesh copper grids. Fig. 2(a) is a low magnification electron micrograph showing several embedded fibres in a 100 nm thick section. Fig. 2(b) is an electron micrograph at higher magnification of a single fibre. A fibre diameter of 10 μm is measured, which is slightly larger than that determined from Fig. 1, probably due to the non-circular cross-section of the

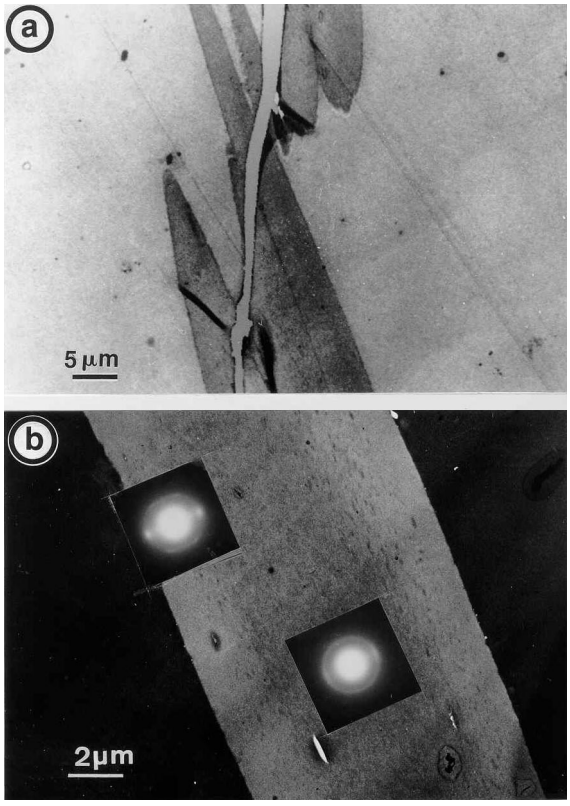

Fig. 2. TEM image of a longitudinal cross-section of a bundle of Fibro® fibres: (a) low dose and low magnification image; in this image, the resin appears clear and the sample dark; (b) same as in (a), but image of one fibre after extensive irradiation: in this image, the resin appears darker than the fibre. The darker core region in the fibre corresponds to less dense area. Inset: typical electron diffraction patterns of the skin (left) and the core (centre) recorded on one square micron of the specimen.

fibre. Skin and core regions can be clearly distinguished. With the contrast that was used to record this figure, the core of the fibre appears less dense than the skin. In addition, there are a number of elongated voids in the skin, with a maximum void concentration near the skin/core interface. In this figure, the thickness of the skin layer is estimated at approximately 2 μm.

2.2. Electron diffraction experiments

The thin sections of Fibro® fibres were analysed with a Philips CM 200 CRYO transmission electron microscope (TEM) operated at 200 kV under low dose conditions. Selected area electron diffraction diagrams were recorded on a specimen diameter of 1 μm. An electron dose of around 200 electrons/nm^2 was used to obtain the diffraction patterns from virgin areas of the specimens. This dose was sufficient to record one diagram on Agfa Scientia films; however, beyond this recording the sample did not diffract any more.

2.3. X-ray microbeam diffraction experiments

The X-ray microbeam diffraction experiment was carried

out on beamline ID13 (Microfocus) at the European Synchrotron Radiation Facility (ESRF) at an X-ray energy of 15.8 keV (wavelength 0.079 nm). An ellipsoidal mirror and a tapered glass capillary focussed the monochromatic beam down to a diameter of 2 μm (width at base) at the exit of the capillary with a beam divergence of 2.3 mrad. A circular platinum–iridium guard aperture of 20 μm in diameter reduced diffuse scattering from the capillary exit well. At the sample position (0.5 mm away from the capillary exit), the beam diameter was approximately 2 μm (FWHM) and the total flux 10^{10} photons/s (see Ref. [6] for more details on beamline set-up). A beam stop of diameter 1 mm was placed at 20 mm behind the sample and the detector was positioned at a pre-calibrated distance of 46 mm. An image-intensified CCD detector with video-readout was used (768 × 576 pixels of size 126 × 126 μm^2).

The metal ring holding the sample (see Section 2.1.) was mounted on a goniometer head and optically pre-aligned. The goniometer head was placed on a high precision *x*/*y* translation stage. Here, the fibre was positioned in the centre of a high-resolution microscope with a precisely known offset to the X-ray beam. With this calibration, it was possible to scan reproducibly across the fibre. Perpendicular to the fibre axis, the step size was 2 μm in a range of ±10 μm with respect to the fibre centre. At six of these 11 points, a diffraction signal from the fibre was detected. Fig. 1 schematically shows these six positions of the beam. Three scans of this kind were carried out with an offset of 10 μm each along the fibre axis. At each position, 800 frames of 40 ms were accumulated. The three diffraction patterns from individual scans but at the same lateral position were found identical and they were summed up in order to improve counting statistics. During the 32 s of total exposure to the X-ray beam at each position, no intensity decay of the diffraction pattern due to beam damage was observed. Thus, the stability of cellulose at the presently used higher X-ray energy (15.8 keV) is higher than that at 13 keV [9].

All data analysis (background correction, radial and azimuthal integration) was carried out using the FIT2D software package [10].

3. Results

3.1. Electron diffraction

As already mentioned in the previous section, an electron micrograph of a thin section of Fibro® fibre (Fig. 2(b)) gives evidence for significant structural differences of a 2 μm thick skin layer and core structure. Electron diffraction experiments confirm this finding: the insets in Fig. 2(b) show two electron diffraction diagrams from selected areas of the fibre section. The background around the primary beam, arising from inelastic scattering, is considerably high, and the diffraction signal comparably weak. Therefore, just the strong equatorial reflections and the second layer line are visible. It should be noted that despite the small illuminated area of 1 μm in diameter, the two diffraction patterns do not indicate any deviations from the perfect fibre texture of the crystalline cellulose microfibrils. Even close to the fibre edge there seems to be no preferred orientation of the crystallites with respect to the surface of the fibre.

The second qualitative result concerns the degree of alignment of the microfibrils with the fibre axis. The equatorial reflection in the diffraction patterns from the skin layer are well-defined spots, whereas the core pattern shows arcs extending largely in the azimuthal direction of the fibre diagram. However, due to the limited signal-to-noise ratio of the electron diffraction patterns, no quantitative evaluation of the degree of orientation could be carried out. This was one reason for performing position-resolved X-ray diffraction experiments on a single Fibro® fibre although, using an entire fibre instead of a thin section, one cannot directly discriminate surface layer and core of the fibre.

3.2. X-ray microdiffraction

The grey-shaded area in the bottom part of Fig. 3 gives the integrally scattered intensity at the six positions (2 μm lateral separation) on the fibre, which are schematically depicted in Fig. 1. The position dependence of the intensity indicates a non-circular fibre cross-section. The asymmetry corresponds well with the serrated outline of the fibre (see SEM image in Fig. 1).

X-ray diffraction diagrams from positions 1 and 4 are presented as insets in Fig. 1. The indexed diffraction pattern (according to Ref. [11]) from the edge position (1) is found in Fig. 4(a) (label “skin”). In contrast to the electron diffraction diagrams, the inner $1\bar{1}0$ equatorial reflection and the third and fourth layer line are clearly visible. Even the neighbouring 110 and 020 reflections may be visually

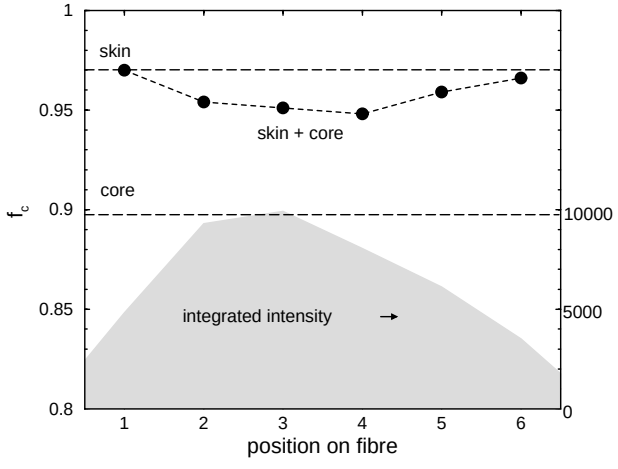

Fig. 3. Position-dependent parameters obtained from X-ray diffraction diagrams: integrated scattered intensity (grey-shaded area, right scale), degree of orientation (f_c) of crystalline regions (full circles, left scale). The dashed lines indicate the degree of orientation of pure skin and pure core, respectively.

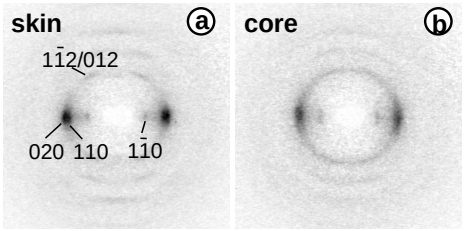

Fig. 4. X-ray microdiffraction patterns of (a) rayon skin and (b) core parts; (a) is the same image as shown in Fig. 1 at the fibre edge (position 1). Indexation is according to Ref. [11]; (b) was calculated from the images at positions 4 and 1 with the assumption of a 2 μm thick skin (for more details see the text).

separated. The two diagrams in Fig. 1 are normalised with respect to their differing integrated intensity (see Fig. 3). They are significantly different: the angular (azimuthal) extent of all visible reflections is much smaller at the very edge of the fibre (position 1) than in the central part (position 4).

At first view, the skin/core effect is less striking than in the case of electron diffraction (Fig. 2(b)). The reason for this is that a diffraction pattern from the fibre centre always represents a superposition of the signals from core and skin. The core/skin volume ratio can be roughly estimated: assuming a skin layer of 2 μm thickness and a fibre of circular cross-section with a diameter of 9 μm, the ratio should be around 5/4. With the same assumption, the edge pattern from position 1 (Fig. 4(a)) is a "pure skin" diagram as beam size and skin layer thickness are identical. Applying the scaling proposed above, it is now possible to obtain a "pure core" diffraction diagram (Fig. 4(b)) by taking the difference of the diffraction patterns inserted in Fig. 1. The difference diffraction diagram (Fig. 4(b)) shows a substantially larger "arcing" of the reflections than the diagram from position 4 (inset in Fig. 1). Comparing finally Fig. 4(a) and (b) (skin and core), their difference is as pronounced as that of the electron diffraction patterns (Fig. 2(b)): that of skin material is characterised by relatively sharp reflections, whereas in the core structure the arcs of the 110/020 equatorial reflections and of the second layer line are merging. The X-ray microdiffraction diagrams from the six positions on the fibre as well as the core pattern from Fig. 4(b) were subject to a quantitative analysis in terms of *crystallite size*, *crystallinity* and *orientation*.

3.3. Crystallite size and crystallinity

The analysis of lateral crystallite sizes and crystallinity was based on radially integrated diffraction patterns. Circular "cake" sections in the range of ±15° with respect to the equator were rebinned to 2Θ scans in order to yield one-dimensional diffraction diagrams of the three strong *hk*0 reflections. Besides the different overall scaling (integrated intensity), these patterns are quantitatively identical within the error at all the six positions on the fibre. Apparently, the skin/core effect is not due to changes of size and structure of the crystalline areas. Their common properties inside skin and core will be summarised below in detail.

A full-profile fit of these scans containing the strongly overlapping 110 and 020 reflections is very sensitive to the choice of the correct peak profile, which is in principle not known. According to the findings in Ref. [12], a pseudo-Voigt profile (i.e. a linear combination of Gaussian and Lorentzian) was chosen for the Bragg peaks, the amorphous background was modelled by a third-order polynomial. Generally, reflection widths could be determined with higher precision than their position. In the fit of the three equatorial reflections, the lattice parameters *a*, *b* and γ were refined. Within the error, they are in agreement with the crystal structure of cellulose II found in the literature [11,13,14].

From the reflection widths of the three strong equatorial reflections, apparent lateral particle sizes were calculated using the Scherrer formula. We obtained 4.8(4) nm along the direction perpendicular to the (1$\bar{1}$0) planes, 2.7(2) and 2.9(2) nm perpendicular to (110) and (020) planes, respectively. Hence, the microfibrils consist of some 10 unit cells in the cross-section (*ab*-plane), which gives a mean diameter of ordered regions of the order of 4 nm. This size estimation has to be regarded as a lower limit as additional broadening effects have not been taken into account. Within the error, the size is the same for skin and core.

Sisson [3] concluded from electron microscopic studies that the skin is composed of smaller, less perfect crystalline areas: he specified that the lengths of cellulose crystallites were of 10 nm in the skin, but 20 nm in the core. This is not contradictory to our results as we measured only the lateral size (width) of the microfibrils. These seem to be less wide than long since the weak 00*l* (meridional) reflections are relatively sharp in radial direction. To determine the exact crystallite length by means of X-ray diffraction the fibre would have had to be tilted by the Bragg angle of a meridional reflection in order to enhance its intensity. This was, however, impossible with the present experimental set-up.

A relative measure of crystallinity, i.e. the amount of crystalline cellulose, was obtained by comparing the integrated intensity of the Bragg peak and of the amorphous background (see Ref. [12]). This ratio fluctuates by ±3% depending on the position; however, there is no systematic variation from skin to core.

3.4. Orientation

For a detailed analysis of the orientational distribution of the cellulose II crystallites, the diffraction diagrams were integrated radially at the positions of the 020 and the 1$\bar{1}$0 reflections. Fig. 5 shows such azimuthal intensity distributions of the 020 reflection for two different positions (1 and 4) on the fibre. The scans contain some intensity from the second layer line reflections 1$\bar{1}$2 and 012, which correspond to slightly smaller 2Θ values. The fit region to obtain the

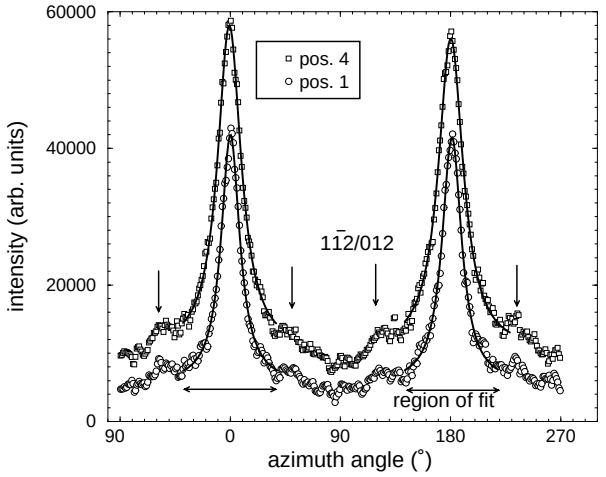

Fig. 5. Azimuthal intensity distribution of the equatorial 020 reflection of the X-ray diffraction diagrams in Fig. 1 The curves were fitted using Lorentzian profiles, however, only in the marked regions in order to exclude the contribution of the 1$\bar{1}$2 and 012 reflections (arrows). The values of the reflection widths are found in Table 1.

azimuthal width of the 020 reflection was, therefore, restricted as indicated by the bars in Fig. 5. Two Lorentzian-shaped peaks (and a constant background) fit the curves well (continuous lines in Fig. 5). Fits of this quality were obtained for all the six positions on the fibre as well as for the "pure core" diffraction diagram from Fig. 4(b). The resulting 020 peak widths are displayed in Table 1. The respective fits of the azimuthal 1$\bar{1}$0 reflection profiles lead to similar but—due to limited counting statistics—less precise results.

In principle, the azimuthal orientation distribution of the 020 planes is not the desired information on misalignment of microfibrils with respect to the fibre (*c*-) axis; it would rather be contained in the azimuthal profiles of meridional (00*l*) reflections. As already mentioned, the latter were too weak to be analysed quantitatively. However, in the case of the presence of (1) a *c*-axis perpendicular to the *ab*-plane and (2) an ideal fibre texture—which is very likely in the case of Fibro®, see Section 2—the azimuthal widths of equatorial and meridional reflections are believed to be identical. The degree of orientation, f_c, is directly obtained from the azimuthal widths according to $f_c = (3\langle\cos^2\phi\rangle - 1)/2$ [15]; ϕ is calculated from the azimuthal full-width at half-maximum (fwhm) according to $\phi = \text{fwhm}/2\sqrt{2\ln 2}$. The resulting degrees of orientation range from 0.97 (skin) to 0.90 (core) (see Table 1). The position dependence of f_c (Fig. 3, upper part) confirms the qualitative findings from the two-dimensional diffraction diagrams. The Fibro® rayon fibre possesses a 2 μm thick skin with a high orientation of the cellulose II crystallites with respect to the fibre axis. The core regions are much less oriented; the values of f_c from the more central parts of the fibre are significantly smaller than that at the edges. This means that the contrast between pure skin and a superposition of skin and core diffraction signals is sufficient to be detected with X-ray microdiffraction of a single, entire fibre.

Table 1
Results of X-ray diffraction mapping. Azimuthal widths (fwhm) of the 020 cellulose II reflections at different positions of the Fibro® fibre (see Fig. 1) are given in column 2, the corresponding degree of orientation in column 3. The position "core" denotes the difference diffraction diagram in Fig. 4(b)

Position (see Fig. 1)	fwhm of 020 reflection (°)	Degree of orientation (f_c)
1 (skin)	19.2	0.979
2	23.8	0.954
3	24.4	0.951
4	25.2	0.948
5	22.4	0.959
6	20.4	0.966
(core)	35.7	0.897

4. Discussion and conclusions

The two mapping techniques presented in this work provide information on the microstructure of fibres with microscopic position resolution. There are, however, considerable differences to be discussed concerning sample preparation, experiment and data analysis: The embedding and sectioning technique for electron diffraction samples is destructive and time consuming. In the case of X-rays, entire fibres are readily investigated, at the expense of the impossibility to investigate "pure core" material; this turned out to be no problem if there are significant differences between skin and core structures. The instrumental efforts for both techniques are non-negligible. They are even higher for X-ray microdiffraction as high-brilliance synchrotron radiation is required; on the other hand, the X-ray experiment may be performed within half an hour, including sample preparation and alignment, whereas the time to obtain electron diffraction results is considerably longer. As the latter are in addition very difficult to be analysed quantitatively—due to the strong interaction of electrons with matter—X-ray microdiffraction is favourable for morphological investigation of fibrous polymers with respect to selected-area electron diffraction. The X-ray microbeam is a fast and non-destructive probe for the investigation of single polymer fibres. Furthermore, the method is not only restricted to microdiffraction mapping but position-resolved micro small angle scattering (μSAXS) is possible as well [9,16]. For example, μSAXS mapping experiments on PET fibres indicate a higher concentration of pores in the core of these fibres [16].

The main result of our studies concerning the skin/core structure of viscose fibres is the finding that the skin is characterised by the presence of voids (on the microscopic scale) and a much higher orientation of the crystalline regions (on the nanoscale). There is no evidence for a significant difference in crystallinity and mean crystallite

size between skin and core. The high alignment of the cellulose chains in the skin layer appears to be the main reason for the higher macroscopic strength of viscose rayon yarns possessing a skin.

Acknowledgements

The authors would like to thank M. Burghammer (ESRF) for his help in setting up the synchrotron experiment, and I. Snigireva (ESRF) for the preparation of SEM images of rayon fibres (Fig. 1). The Fibro® fibres were kindly supplied by I. Graveson from Courtaulds Research and Technology.

References

[1] Morehead FF, Sisson WA. Text Res J 1945;15:443.
[2] Preston JM. J Soc Chem Ind 1931;50:T199.
[3] Sisson WA. Text Res J 1960;30:153.
[4] Haase J, Hosemann R, Renwanz B. Kolloid-Z Z Polymere 1973;251:871.
[5] Lenz J, Schurz J, Wrentschur E, Geymayer W. Angew Makromol Chem 1986;138:1.
[6] Riekel C, Cedola A, Heidelbach F, Wagner K. Macromolecules 1997;30:1033.
[7] Hagege R. In: French AD, Gardner KH, editors. Fiber diffraction methods, ACS symposium series A, 41, 1980. p. 279.
[8] Bachhuber K, Frösch DJ. Microscopy 1982;130:1.
[9] Müller M, Czihak C, Vogl G, Fratzl P, Schober H, Riekel C. Macromolecules 1998;31:3953.
[10] Hammersley AP, Svensson SO, Thompson A. Nucl Instrum Meth A 1994;346:312.
[11] Kolpak FJ, Blackwell J. Macromolecules 1976;9:273.
[12] Hindeleh AM, Johnson DJ. Polymer 1974;15:697.
[13] Stipanovic AJ, Sarko A. Macromolecules 1976;9:851.
[14] Raymond S, Kvick Å, Chanzy H. Macromolecules 1995;28:8422.
[15] Stein RS, Wilkes GL. In: Ward IM, editor. Structure and properties of oriented polymers, London: Applied Science Publishers, 1975. p. 57.
[16] Riekel C, Engström P, Martin CJ. Macromol Sci—Phy B 1998;37(4):587.